Space Resolved Optical Emission Spectroscopy of $Ni(CO)_4$ Interaction with a Cold Remote Nitrogen Plasma

A. Brocherieux, P. Supiot, O. Dessaux and P. Goudmand

Laboratoire de Physico-Chimie de l'Energétique et des Plasmas
(E.A. M.R.E.S. n°1761) Université des Sciences et Technologies de Lille
F - 59655 Villeneuve d'Ascq Cedex - **France**

Abstract
A spatially resolved optical emission spectroscopic study of the flame resulting from the $Ni(CO)_4$ decomposition in a Cold Remote Nitrogen Plasma is presented. A kinetic analysis is carried out and correlated to metallic nickel deposition.

Introduction

The present work deals with the gas phase spectroscopic study of the interaction of a Cold Remote Nitrogen Plasma with the $Ni(CO)_4$. This molecule is of interest for metallic nickel deposition. Different trends for its decomposition have already been followed leading either to metallic or powdered nickel according to experimental conditions : the thermal processes [1], the laser CVD [2,3,4,5] and of course the RPECVD in dinitrogen [6]. Some kinetic models are proposed to account for the decomposition chemistry in each process either from the study of the deposit [1,2,4,6] or from the gas phase spectroscopic properties in the laser process [5]. For plasma applications, only the interaction of $Ni(CO)_4$ with metastables of Ne, Ar and He [7] and with dinitrogen [8] have been studied by optical emission spectroscopy, but the complete decomposition mechanism is not still undertsood. Here we present some results on the spatial structure of the flame via the monotoring of some specific emissions. Besides, we discuss the reaction scheme proposed by Brennen [8] and try, for the first time, to correlate the spectroscopic results with the deposit characteristics.

Experimental

A 2450 Mhz resonant cavity [9] generates a nitrogen flowing plasma at a pressure of 5.8 hPa (corresponding flow rate : 2.58 slpm). The transmitted power is equal to 800W. The flowing plasma is led to a reaction chamber, 230 cm downstream the discharge. At the entrance of the chamber (150 mm diameter), it is confined in a glass

tube (40 mm diameter) as far as 20 mm upper the optical axis. The nickel tetracarbonyl gas is injected colinearly to the plasma flow and inside the confining tube (Fig. 1). The $Ni(CO)_4$ flow rate, not measured for this work, is less than 2 sccm and controlled by a microvalve. A conic reaction area appears with diameter equal to ~ 20 mm at the optical axis level. The spectroscopic and spatial distribution analysis is carried out along the reactor diameter, in the plane of the optical axis at right angle to the flow axis and at about 50 mm downstream from the $Ni(CO)_4$ injection. The emission signal is collected through a BK7 window and a diaphragm (5 mm diameter) and is transmitted to a THR-1000 Jobin-Yvon monochromator equipped with a multichannel detection head. Emissions are studied in the 350-700 nm spectral range with an entrance slit of 300 μm. A mathematical treatment (Abel inversion) [10] allows to determine for each emitter the radial distribution of the emissivity $\varepsilon_\lambda(r)$ from the global intensity I(y) recorded on the line of sight x (Fig. 1) : $\varepsilon_\lambda(r) = -\frac{1}{\pi}\int_r^{r_0} \frac{I'(y)dy}{\sqrt{y^2 - r^2}}$ where I'(y) is the derivation of I(y). Besides, the set of the recorded values I(y) is represented by cubic splines functions. To account for the relative concentrations of the different emitters, I(y) is divided by the spectral response of the optical apparatus and by the transition probability at the given λ value (table I). The calculated $\varepsilon_\lambda(r)$ quantity can hence be meant as the local relative concentration of the considered emitter (denoted [emitter]). The Abel inversion assumes, of course, a cylindrical symmetry. This condition is not always strict fulfilled, so an average I(y) profile is calculated (Fig. 2a - $\langle I \rangle(y)$: continuous and high lines). Then, the Abel inversion has been carried out from these mean values $\langle I \rangle(y)$ (Fig. 2 - $\varepsilon_\lambda(r)$: continuous and low lines).
Otherwise, to visualise the spatial distribution of the deposit, a rectangular plate has been vertically positioned near the observation zone. It is centered on the flow axis and perpendicular to the optical axis. The deposit is hence collected with the smallest perturbation of the flow in the reaction cone area.

Results

The observed emissions in the reaction area are mainly generated by the atomic emitters of nickel, the numerous emission lines of nickel cover an important energy range : from 3.30 eV ($z^5D^0 \equiv 26666\ cm^{-1}$) to 6.72 eV ($g^3F \equiv 54251\ cm^{-1}$). The Lewis-Rayleigh emission of N_2 ($B^3\Pi \rightarrow A^3\Sigma$) and the violet and red systems of CN ($B^2\Sigma \rightarrow X^2\Sigma$; $A^2\Pi \rightarrow X^2\Sigma$) also appear. Neither NO or CO emissions nor that of $Ni(CO)_3$ continuum [11] are significantly detected under our experimental conditions. The table 1 presents the recorded transitions for the spatial study, chosen in well discriminated spectral regions and spread in energy.

Radial distribution of different emitters

The resulting profiles are shown on figure 2a. The emissivity $\varepsilon_\lambda(r)$ maximum obtained by the Abel inversion is set at about 1 cm from the injection axis for all the emitters.

This signifies that in the observation plane, the greatest density of the emitters is settled in the same ring centred around the injection axis. At the centre, the density of emitters is close to zero. Moreover, no emitter is detected beyond 2 cm from the injection axis. One can notice that the width at half maximum $\varepsilon_\lambda(r)$ value is less for Ni emitters than for $N_2(B^3\Pi)$ state.

Table 1 : Analysed transitions

Emitter	Transitions	Wavelength (nm)	Energy (eV)	Transition probability (10^8 s^{-1})
Ni	$e^5F \rightarrow z^5G^0$	471.4	6.01	0.46
	$z^1D^0 \rightarrow a^3P$	631.6	3.90	0.0057
N_2	$B^3\Pi \rightarrow A^3\Sigma$ (second band head of (11,7))	579.7	9.70	0.001

Deposition

As shown by the figure 2b, the metallic nickel occurs at a radius value close to 1 cm, in a region which is 1 cm large. Inside this area, powdered nickel is present. Metallic nickel seems in coincidence with a maximum concentration of nickel emitters.

Discussion

The figure 2a allows the study of the variations of Ni* density, [Ni*], versus that of $[N_2(B^3\Pi)]$. With regard to the $[N_2(B^3\Pi)]$ profile, two distinct areas are defined : the center of the reaction cone where $[N_2(B^3\Pi)]$ is minimum and the external zone beyond the position of its maximum value. A resulting dependence of [Ni*] on $[N_2(B^3\Pi)]^n$ for both e^5F and z^1D^0 states is observed in the both regions. The deduced n value is in the interval $5/2 \leq n \leq 3$ for the the first region and equal to 3 in the second one. If no further significant quenching of the $N_2(B^3\Pi)$ state occurs in the reaction with $Ni(CO)_4$ (low carbonyl pressure), the resulting intensity of the $N_2(B^3\Pi \rightarrow A^3\Sigma)$ is proportional to the square of N atom concentration,[N]. On the basis of the assumption, the dependence of [Ni*] versus [N] is hence to the power 5 to 6. The interaction of $Ni(CO)_4$ with nitrogen plasma has been explained by a sequential and stepwise degradation [8]:

$$Ni(CO)_n + N \rightarrow Ni(CO)_{n-1} + NCO \quad (1)$$

$$Ni + N_2(A^3\Sigma) \rightarrow Ni^* + N_2 \quad (2)$$

The reaction of type (1) involves four N atoms for the production of one Ni atom. Furthermore two further N atoms are required for $N_2(A^3\Sigma)$ creation. The Ni* excitation is hence possible after reaction of six N atoms on $Ni(CO)_4$. The mechanisms (1) and (2) imply a significant stability of the intermediate species and high collisional rate, and hence the control of the Ni* concentration by that of N. This dependence is in

good accordance with our results. That also assumes an excess and no strong radial gradient in $Ni(CO)_4$ concentration with regard to that of N atoms everywhere in the reaction zone. An analogous study achieved at low $Ni(CO)_4$ flowrate supports this result. Indeed, under the latter conditions, the presence of $N_2(B^3\Pi)$ at the center of reaction cone suggests a stronger gradient of $Ni(CO)_4$ concentration and no clear dependence is appeared between the emitters. This fact added to the. The n value, leading to a five or six steps sequence, is supported by proven existence of $Ni(CO)_n$ ($n < 4$) fragments [5,11]. Nevertheless, the $Ni(CO)_3$* luminescence continuum (centered at $\lambda \sim 650$ nm) is not observed in our experiment because of an important degradation rate due to collisions with N atoms.

The analysis of Brennen [8] is somewhat in contradiction with its experimental results. The latters indicate a quadratic dependence of the global intensity of its $Ni(CO)_4$ flame on that of the $N_2(B^3\Pi \rightarrow A^3\Sigma)$ transition. The discrepancies with our data are well explained by the difference between the global recorded intensity and the emissivity $\varepsilon_\lambda(r)$ which is directly related to the local species concentration. Indeed we have also observed a similar quadratic relationship between the intensities (I(y=0)) for Ni* and $N_2(B^3\Pi \rightarrow A^3\Sigma)$ transition, while [N] is varying with the microwave power. The data of Brennen give only a spatial and spectral average description, while our work is established on local species concentration.

On the basis of reaction (1), the production of NCO, which can be decomposed by various ways [8] leading to CO and NO fragments, should result in emissions from these latters. The absence of CO and NO emissions could be explained by their destruction through the following reactional scheme :

$$N_2(B^3\Pi) + CO(X^1\Sigma) \rightarrow CN^* + NO(X^2\Pi) \quad [12] \quad (3)$$

$$N + NO(X^2\Pi) \rightarrow N_2 + O \quad [13] \quad (4)$$

The reaction (4) is very efficient ($k_4 = 2.7 \times 10^{-11}$ $cm^3.s^{-1}$). The reaction (3) could additionally explain the CN emissions.

Otherwise, the simultaneous observation of figures 2a and 2b indicates that the metallic nickel deposition occurs when Ni* concentrations become important. Besides, the nickel powder appears in the central area. Both deposits are generated from the atomic nickel production. The metallic deposit grows on the glass surface in the vicinity of Ni atoms creation zone. Then, the occurrence of powder, which essentially takes place in homogeneous phase, is due to aggregation of Ni atoms with other gas phase partners. In summary, the powder growth requires a long transport time and we can conclude that the observed deposit at the center represents the collection of the upstream producted grains. This analysis is consistent with the experimental results.

Conclusion

The spatial optical emission spectroscopy of the $Ni(CO)_4$ interaction with a Cold Remote Nitrogen Plasma is used to understand the main mechanisms involved in the nickel deposition process. The concentration radial profiles of Ni (e^5F, z^1D^0) and $N_2(B^3\Pi, v=11)$ emitters are established by the Abel inversion method. An original

dependence law of Ni emitters concentration versus that of $N_2(B^3\Pi, v=11)$ is deduced from the recorded data. It leads to an order 6 versus the N atom concentration. A correlation of the concentration profiles is achieved with the deposit features, e.g. the metallic or powdered nature. The Ni excited concentration maximum coincides with the metallic nickel film growth location. This observation gives a good qualitative diagnostic to evaluate and hence to anticipate the optimized position of the substrate for metallic film deposition.

1. H.E. Carlton and J.H. Oxley, A.I. Ch. J. 13,1,86 (1967)
2. J. Tonneau, Appl. Phys., 64, 10 5189 (1988)
3. S. Boughawa and G. Auvert, Appl. Surf. Sci., 69, 79 (1993)
4. E. Borsella, K.L. Kompa, H. Reiner and H. Schröder, Proc. SPIE-Int. Soc. Opt. Eng., 1279 (Laser-assisted Process. 2), 160 (1990)
5. H. Reiner, Ch. Wittenzellner, H. Schröder and K.L. Kompa, Chem. Phys. Letters, 195, 169 (1992)
6. A. Brocherieux, O. Dessaux, P. Goudmand, L. Gengembre, J. Grimblot, M. Brunel and R. Lazzaroni, Appl. Surf. Sci. (1995) to be published.
7. D.C. Hartman, W.E. Hollingsworth and J.S. Winn, J. Chem. Phys. 72, 2, 833 (1980)
8. W.R. Brennen and G.B. Kistiakowsky, J. Chem. Phys., 44, 2695 (1966)
9. C. Dupret, P. Supiot, O. Dessaux and P. Goudmand, Rev. Sci. Instrum. 65, 11, 3439 (1994)
10. M.Deutsch, Appl. Phys. Lett., 42, 3, 237 (1983)
11. N. Rösch, M. Kotzian, H. Jörg, H. Schröder, B. Rager and S. Metev, J. Am. Chem. Soc., 108, 4238 (1986)
12. A.T. Stair, J.P. Kennealy and R.E. Murphy, J. Chem. Phys., 64, 52 (1967)
13. K. Sugawara,Y. Ishikawa and S. Sato, Bull. Chem. Soc.Jpn 53 ,3159 (1980)

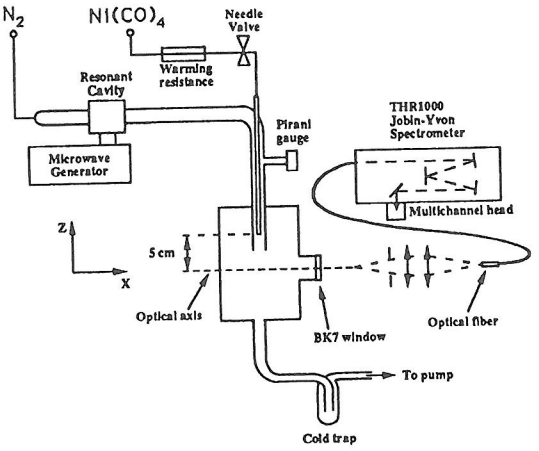

Fig. 1 : Experimental set-up

(2a)

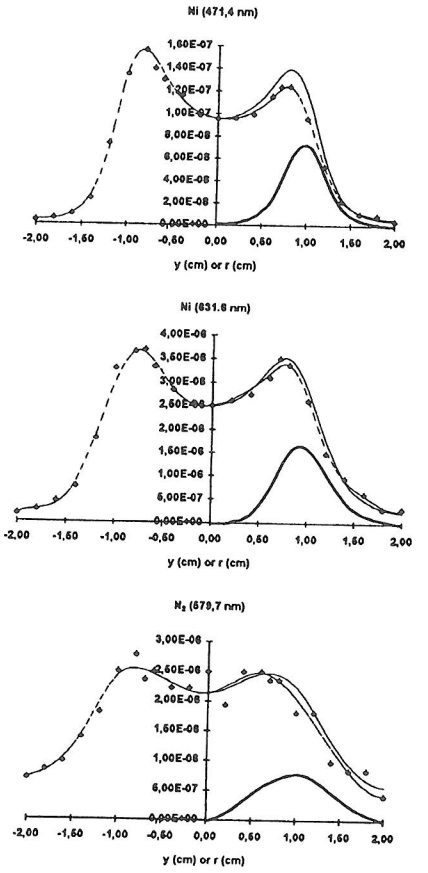

(2b)

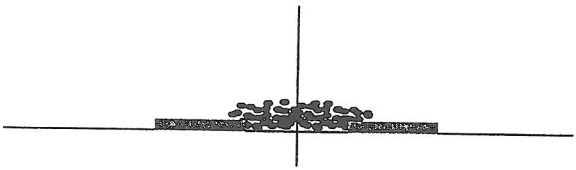

Fig. 2 : (a) Profiles of the experimental intensity I(y) (black diamonds, dotted line), the mean intensity <I>(y) (full line) and the emissivity $\varepsilon_\lambda(r)$ (bold line) observed along the reactor diameter, (b) Deposit features : (grey) metallic nickel, (•) powdered nickel.